Microsyst Technol (2014) 20:1023–1033
DOI 10.1007/s00542-014-2104-0

TECHNICAL PAPER

A microbial fuel cell powering an all-digital piezoresistive wireless sensor system

T. Tommasi · A. Chiolerio · M. Crepaldi · D. Demarchi

Received: 14 August 2013 / Accepted: 26 January 2014 / Published online: 9 February 2014

Abstract Microbial fuel cells (MFCs) are energy sources, which generate electrical charge thanks to bacteria metabolism. We report on a full custom pressure wireless sensor node especially designed to operate with MFCs, comprising an ultra-low-power Impulse-Radio Ultra-Wide-Band Transmitter operating in the low 0–960 MHz band, a nanostructured piezoresistive pressure sensor connected to a discrete component digital read-out circuit, and an MFC energy supply system. The sensor device comprises an insulating matrix of polydimethylsiloxane and nanostructured multi-branched copper microparticles as conductive filler. Our prototype system comprises two MFCs connected in series to power both the UWB transmitter, which consumes 40 μW, and the read-out circuit. The two MFCs generate an open circuit voltage of 1.2 ± 0.1 V. Each MFC prototype has a total volume of 0.34 L and comprises two circular poly(methyl methacrylate) chambers (anode and cathode) separated by a cation exchange membrane. The paper reports measurements on a fully working prototype that enables the separate transmission of pressure information and MFC voltage level at the same time. The complete sensor node powered by the MFC, thanks to its nature can be located either in harsh environments where there is no connection to energy grids, or in environments where the MFC, hence the complete node, can self-sustain.

T. Tommasi (✉) · A. Chiolerio · M. Crepaldi · D. Demarchi
Center for Space Human Robotics, Istituto Italiano di Tecnologia, Corso Trento, 21, 10129 Turin, Italy
e-mail: tonia.tommasi@iit.it

A. Chiolerio
e-mail: alessandro.chiolerio@iit.it

M. Crepaldi
e-mail: marco.crepaldi@iit.it

D. Demarchi
Department of Electronics and Telecommunications (DET), Politecnico di Torino, Corso Duca degli Abruzzi, 24, 10129 Turin, Italy
e-mail: danilo.demarchi@polito.it

1 Introduction

In recent years, research on wireless sensor networks (WSN) gained significant and progressive importance. WSN can be used for continuous monitoring and on-line control in a wide range of applications, in particular for real-time data acquisition from remote locations (Donovan et al. 2008), environmental monitoring e.g. biosensor for wastewater (Di Lorenzo et al. 2009), oceanographic studies (Reimers et al. 2006) and military surveillance (Park and Ren 2012) using underwater acoustic sensors (Akyldiz et al. 2005). Despite a significant performance increase for electronic components, functionality of remote wireless sensors is limited by power source capabilities. Traditionally, wireless sensors are powered using dry cell batteries (Diamond et al. 2008), although their use is problematic for their limited lifetime. In remote locations, battery replacement is costly, time consuming and impractical (Donovan et al. 2008). Power requirements hence are a critical issue, also because achieving the long-term operation of remote devices is a challenge. A possible attractive alternative solution to this problem comes from an interesting green technology, i.e., Microbial fuel cells (MFCs). MFCs do not require traditional fuel supply, as in common fuel cells, because electrons generation is based on microbial metabolism. In natural environments indeed (e.g. marine water and river sediment) nutrients are available in the form of oxidized organic carbon, which could serve as fuel for the microbial consortia living into the MFC. Moreover MFCs do not need to be recharged or replaced after exhaustion, as it happens for lithium ion batteries. Although

MFC power rating at their actual development state is not enough for high energy demands, their application can be effective to power sensors and communication system either in harsh environments or remote terrestrial areas, e.g. underwater and in space explorations where human operation is either difficult or impossible, or alternatively to implement complex systems where their operation is a function of the external environmental conditions. The most recent MFCs generate a maximum cell potential of around 0.5–0.8 V and maximum powers in the order of magnitude of some W m^{-2} (Logan 2010; Cheng and Logan 2011). Higher open-circuit voltages of 1 V have also been reported for individual small-scale MFCs under particular conditions (Jong et al. 2006), close to the theoretical maximum of 1.14 V (Ren et al. 2012). This voltage level is indeed enough to power a communication chip. In a wireless network, in general several transceiver (transmitter and receiver) nodes, implemented onto a single silicon chip in a complementary metal oxide semiconductor (CMOS) technology process (in a 130 nm process nominal voltage level is indeed 1.2 V) operate at the same time aiming at exchanging sensor data for monitoring purposes. To generate a sufficient power and reach enough voltage level and supply those wireless communication chips, either scale-up a single unit or to connect multiple small units together is required. Wireless microelectronic systems, especially during the last decade, have gained superior attention for a wide range of applications, and depending on the specific application domains, systems can be very differently constrained. As a consequence and matter of fact, short-range ultra-low-power (ULP) transmitters and receivers can be applied to wireless body area networks (WBAN), WSN and for ubiquitous networking applied to Internet of Things (IoT). Thanks to the CMOS technology process and Radio Frequency CMOS design, a microelectronic system can be aggressively scaled down to meet ultra-small form factors and enable wireless connectivity to a huge range of objects. Among the available wireless technologies, Impulse Radio Ultra-Wide-Band (IR-UWB) attracts the research community thanks to its ultra-low power features combined to ease of implementation and low-complexity. IR-UWB enables the lowest consumed power at the transmitters (TX) compared to any other wireless technology (Crepaldi et al. 2012), because it needs to operate only for a very small portion of time compared to symbol rate (about a factor 1/1,000). In the US, (see the FCC Rules Part 15, subpart F) a signal which can be classified as Ultra-Wide-Band requires a fractional bandwidth of at least 0.2 or bandwidth of at least 500 MHz. In a common wireless technology indeed a TX power amplifier subsystem which steers a low impedance antenna needs to be powered on for a complete symbol duration (where symbol is typically referred to the meaning of the transmitted information, e.g., for digital communication systems, '0' or '1') and kept active longer than in IR-UWB, where pulse duration is only of few nanoseconds. Moreover, an IR-UWB wireless transmission is unlicensed by definition, therefore constrained only by the maximum radiated power levels at the TX, disregarding other wireless systems emission limits and other hard constraints on modulation pulse-to-pulse timing. A train of UWB pulses can always be radiated over-the-air provided that the resulting average Power Spectral Density (PSD) does not exceed the −41.3 dBm/MHz limit. Last but not least, thanks to this impulsive nature, an UWB signal can be easily generated using a small area CMOS integrated circuit, even based only on digital cells, enabling deep miniaturized wireless capabilities within a very small silicon die.

Similarly, in the last decades MEMS technology has matured and corned the market of several application fields. In particular pressure sensors are the most investigated developed and worldwide produced transducers (Eaton 1997). Piezoresistive materials are so that a variation of the material volume induced by a pressure field results in a variation of electrical conductance. In our specific case, a bulk material is used and configured as sensor, providing high sensitivity, low complexity and the capability of operating in harsh environments, if compared to more complex though sensitive MEMS silicon based integrated systems. Typical applications of piezoresistive pressure sensors include automotive, pipes and reservoirs monitoring, industrial and human robotics, smart phones and on line control of analyte concentration in ambient aqueous solutions (Guenther et al. 2010). Among the wide range of materials utilized for piezoresistive devices, the composites based on polymers and metal filler have several advantages, such as flexibility, mechanical robustness, insensitivity to overload, and moreover can be prepared through cost effective processes (Yousef et al. 2011). In the presented application, conduction occurs by tunneling mechanisms in a copper-elastomer composite. As already reported for other metal-polymer hybrid systems with nickel (Canavese et al. 2012a, b), silver (Chiolerio et al. 2013) or gold particle fillers (Stassi et al. 2012a, c), a giant piezoresistive behavior can be obtained, enabling a high sensitivity to a small pressure changes. Based on this relevant piezoresistive behavior, a low-complexity, ULP and all-digital read-out circuit (ROC) can be easily operated to read-out resistance and capacitance variations across these piezoresistive materials. Therefore, the power generated by an MFC can be used to activate a ROC connected to this kind of pressure sensor, which is meant to replicate the human skin sensitivity, and conceived for humanoid robots for space applications.

This work reports the advantages achieved joining these three separate fields, i.e., MFCs, micro-electronics and piezoresistive design, into an energetically sustainable system,

i.e., a wireless sensor node that can be effectively powered by an MFC without requiring energy management and conversion subsystems. The system is conceived so that it suits the operating conditions of an MFC energy source. The paper is organized as follows: Sect. 2 introduces the MFC technology which enables the low-complexity sensor node implementation used in this work. Section 3 introduces the complete wireless sensor node and each subsystem, i.e., the design of the cell, the piezoresistive sensor, the IR-UWB transmitter and the read-out circuit, respectively. Section 4 shows experimental results obtained on the most important subsystems demonstrating system functionality and the feasibility of the idea, plus specific measurement and electrical characterizations of our MFC energy sources; lastly, Sect. 5 concludes the paper.

2 Microbial fuel cells

Many bioenergy conversions exist and include incineration, gasification, fermentation (e.g., bioethanol-based), anaerobic digestion for bio-H_2 and biogas production (Ruggeri and Tommasi 2012). However, MFCs have a number of attractive features such as direct electricity generation, high conversion efficiency, and a reduced production of sludge. Although functionally similar to chemical fuel cells (Müller et al. 2003), i.e., both including reactants and two electrodes, and anode and cathode, they have substantial advantages: (1) operation at ambient temperature and pressure; (2) use of neutral electrolytes and avoidance of expensive catalysts (e.g. platinum); (3) operation using organic wastes. An MFC can be effectively used in environments where ubiquitous networking requires the wireless monitoring of energy sources. According to dimensions, MFCs may be divided into three groups, macro, meso and microscale MFCs. Microbes in the anodic chamber of an MFC oxidize organic substrates fed in the cell and generate electrons and protons in the conversion process. Carbon dioxide is generated as a product of biological oxidation (Fig. 1). Unlike in a direct combustion process, the electrons are attracted to the anode and transported to the cathode through an external circuit. After crossing a cation exchange membrane (CEM) or a salt bridge, the protons enter in the cathodic chamber where they combine with oxygen to form water (Crepaldi et al. 2013a). Microbes in the anodic chamber extract electrons and protons in the dissimilative process of oxidizing organic substrates (Rabaey and Verstraete 2005). Electric current generation is made possible by keeping microbes separated from oxygen or any other end terminal acceptor other than the anode and this requires an anaerobic anodic chamber. That of MFC is an approach that utilizes biomasses after appropriate pretreatments (Ruggeri et al. 2012) and directly generates electricity. The materials used to manufacture electrodes play an important role in an MFC performance (e.g. power output level), energy sustainability and costs. MFC technology can potentially address both energy and water quality challenges because they can enable clean energy production and simultaneous water purification, which generally is very energy-expensive when based on traditional aerobic treatments. The MFC principles have been demonstrated for lab scale devices even though real full-scale applications are currently limited by power yield and long-term performance (Xie et al. 2012).

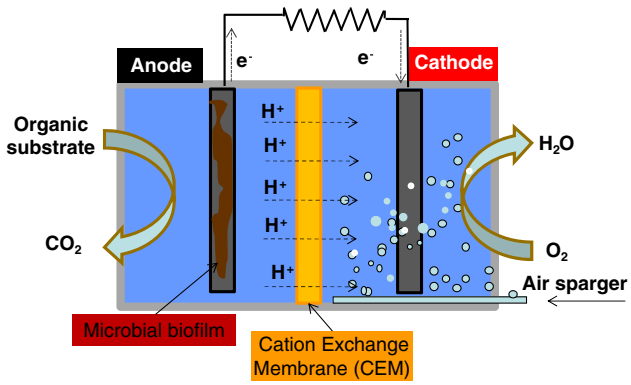

Fig. 1 Schematic diagram of a typical two-chamber MFC (Crepaldi et al. 2013a)

3 MFC-based wireless sensor node concept and subsystems

An MFC can be potentially installed in not easily reachable environments where bacteria flow in the compartments of the cell, can be self-sustained in turn by the environmental conditions where the cell is operating. Even if not suitable for high demands, the MFC can give a large amount of power to dedicated ULP microelectronic systems to run specific and full-custom tasks. We report the block scheme of an all-digital sensor node, which comprises a ROC for pressure information transmission and a circuit sensitive to the power supply to transmit the voltage available across the MFC. Figure 2 shows our system concept block scheme. The node, fully powered by the MFC only, comprises (1) a read-out circuit, a Ring Oscillator (RO), (2) a Time-to-Digital Converter (TDC) for pressure information transmission, (3) a Synchronized-On-Off Keying (S-OOK) modulator (Crepaldi and Demarchi 2013) for digital data transmission and an IR-UWB Transmitter, completely asynchronous to accommodate together both S-OOK, and Pulse Frequency Modulation (PFM) for the transmission of the voltage across the MFC.

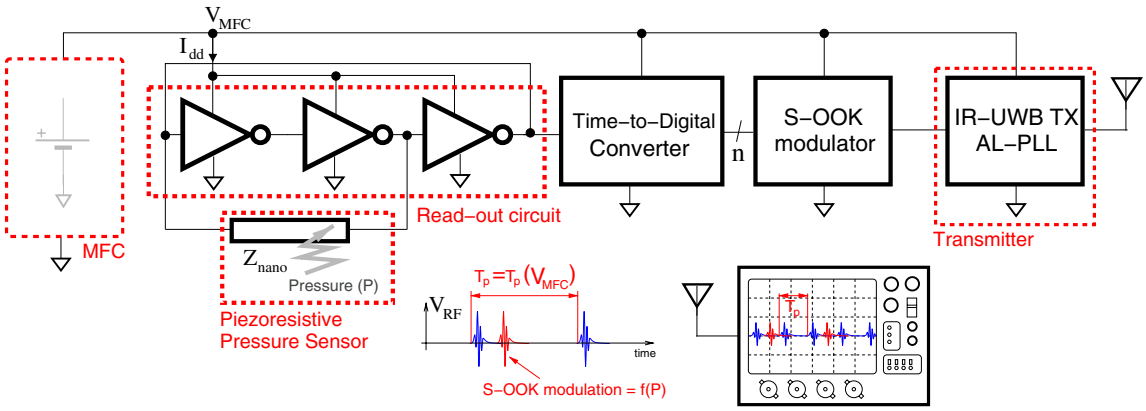

Fig. 2 System concept. An MFC system powers the complete node for pressure sensing, including a read-out circuit, a piezoresistive pressure sensor, a TDC, an S-OOK modulator and an IR-UWB transmitter. Two MFC cells connected in series supply the microelectronic circuit

The energy source depicted in the schematic diagram of Fig. 2 identifies the MFC which provides voltage V_{MFC} and supplies the complete node. The complete system is all-digital, hence voltage and technology scalable: in particular, the whole circuit speed depends on the voltage level with which it is powered on, and it is completely self-synchronized, i.e., each time constant of the circuit is self-correlated through the supply voltage. The system purpose is the simultaneous transmission of both voltage level across the MFC (directly related to the supply voltage conditions of the node) and the pressure information taken from the sensing sub-system, i.e., a nanostructured material. Sensor readout is based on an all-digital, technology and voltage scalable electronic unit as well. The ROC, is indeed a simple all-digital Ring Oscillator (RO), connected to our piezoresistive nanostructured material on which pressure can be applied. The ROC oscillates at a given frequency f_p, period T_p. The steady state frequency of the RO $1/T_p$ depends on the voltage level across its power supply terminals, while the relative frequency variation depends on the resistance and capacitance of the piezosensor, i.e., by the applied pressure. The nominal frequency varies as a function of the resistance and capacitance across the generic impedance (Z_{nano}) because propagation delay of the inverter chain varies, and pressure information is encoded as a variation of the nominal oscillation frequency. This relative variation is converted into digital domain by the TDC. The digital output data asynchronously triggers an S-OOK modulator, which is invoked on-demand based on the TDC event triggers. The S-OOK modulator generates the digital symbols for over-the-air radiation and triggers an asynchronous IR-UWB transmitter. Neither to occupy large spectrum portions nor to jam other existing wireless devices operating in the same spectral range, the TX operates robustly to voltage supply variations, and radiates pulses with accurately controlled center frequency disregarding system voltage supply variations. The RF transmitter then is the only unit that needs to operate robustly to supply voltage variations. Thanks to our all-digital and self-synchronized system architecture, our transmitter node enables the wireless voltage level monitoring across the MFC based on the rate at which the digital S-OOK data is transmitted ($1/T_p$), and at the same time the digital transmission of pressure data without requiring expensive and power demanding electronics, thus maintaining system-level complexity very limited.

The TDC and the S-OOK modulator can be indeed implemented using ULP techniques and do not impact on the concept given in this paper (Crepaldi et al. 2013b) for an ULP implementation of an S-OOK modulator). At the RX side, signal reception is on the other hand enabled by the use of asynchronous energy detection schemes (Crepaldi et al. 2011), which can very easily detect both ($1/T_p$) and demodulate S-OOK digital data to recover pressure information (Motto Ros et al. 2013). Besides these advantages, as a consequence of digitally-enabled modularity, the sensor node can also be tolerant to process variations that may occur when the system is fully implemented in an Application Specific Integrated Circuit (ASIC).

Figure 3 summarizes the communication concept. Thanks to the use of self-synchronized sequences and consequently an all-digital system architecture, both pressure information and MFC voltage level can be still recovered: the RX needs to detect quantity T_p (i.e., directly related to the MFC voltage level) and at the same time demodulate the S-OOK self-synchronized sequences to extract digital pressure data. At different MFC voltage levels indeed the ratio $T_{s\text{-}ook}/T_p$ is maintained constant (self-synchronized), enabling an easy and low complexity demodulation at the RX using an asynchronous energy detector (Crepaldi et al. 2013b).

In this specific paper we focus on the most important sub-systems to demonstrate feasibility and basic operation,

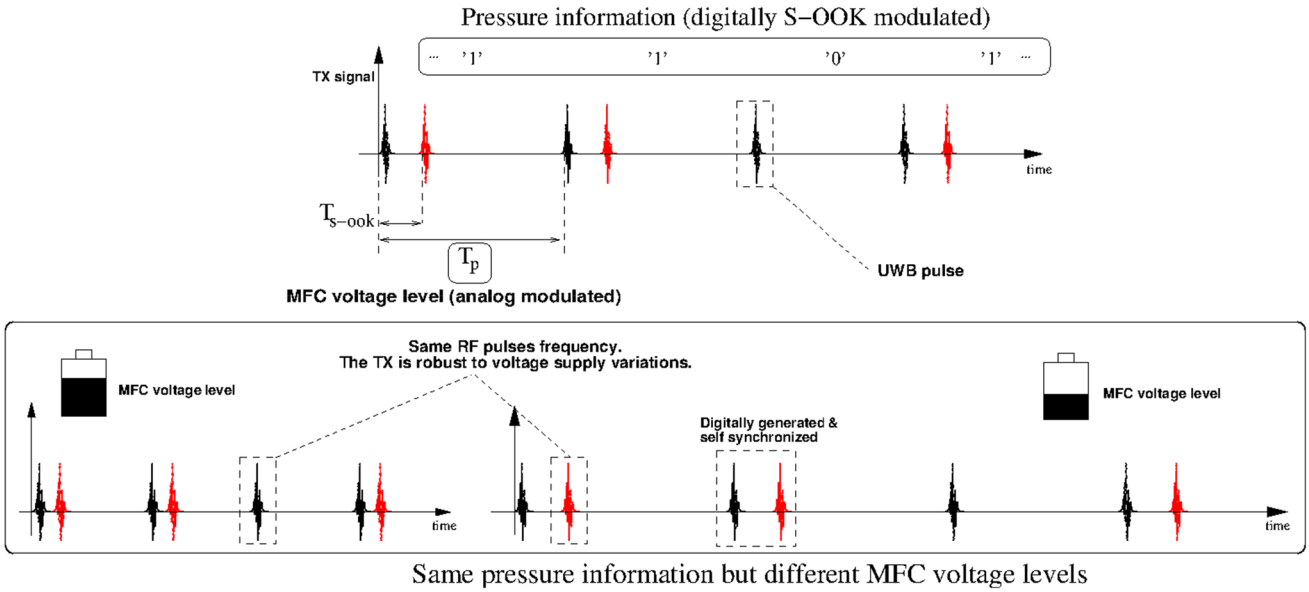

Fig. 3 Communication concept of the complete system. The MFC voltage level is directly related to the S-OOK raw data rate. S-OOK modulated data contains sensed pressure data)

and to show that an MFC although providing unregulated power supply, can successfully power and enable the full operation of our specifically designed sensor node. Hence, we focus only on the most important blocks, which are the IR-UWB transmitter and the read-out circuit.

3.1 Cell design

The MFCs used in this work are designed based on two circular chambers in PMMA with internal diameter of 12 and 1.5 cm of thickness (internal volume for each chamber ~170 mL) separated by a cation exchange membrane (CEM, CMI 7000, Membranes International Inc., Glen Rock, NJ, USA). A carbon cloth (Soft felt SIGRATHERM GFA5, SGL Carbon, Germany) is used as an anode electrode and assembled together with a graphite rod (diameter 2 mm, SGL Carbon, Germany) to ensure an effective current conduction capability. A carbon sheet (CA, USA) joined with a graphite rod is used as cathode electrode.

3.2 Piezoresistive pressure sensor

The piezoresistive sensor used in this work has a large sensor area (10 mm × 10 mm), 1 mm thickness, and it is based on piezoresistive composite material equipped with flexible metalized polyimide electrodes. Specific details about the fabrication process can be find in (Stassi et al. 2012b). In the prepared composite samples, copper particles are intimately coated by a silicone matrix that avoids any physical contact between them. As a consequence, when no mechanical deformation is applied, piezoresistive specimens exhibit an insulating electric behavior due to the insulating silicone matrix (Bloor et al. 2005). During the application of a compressive strain to the functional material, the thin insulating layer between metal particles is compressed and deformed, reducing the average distance among the metallic particles. This fact in turn induces an exponential rise of the electron tunneling probability between neighboring particles. This results in an increase of several orders of magnitude of the sample electrical conductivity. Besides the physics controlling the transduction mechanism, the specific choice of piezoresistive materials was done because of the low cost of the nanocomposite, of the ease in preparing samples, of the soft and conformable nature of polymeric matrix devices, and of the stability in dynamic conditions (Stassi et al. 2012b).

A micro corrugated morphology of the metallic particles helps the polymeric matrix to intimately coat the filler, avoiding physical contact between close particles. Macroscopic flexible skins are produced, whose surface is flat and soft, which may be easily contacted by using metalized Kapton® films, applied from both sides of the material, to allow the continuous resistivity monitoring of the set-up proposed in this paper.

3.3 IR-UWB transmitter

The integrated IR-UWB transmitter used in this work is all digital and it is fabricated in a 130 nm RFCMOS technology process (Crepaldi and Demarchi 2013). Basically it embeds a single-phase charge pump phase locked loop (PLL), which generates an UWB pulse based on a single duty cycling

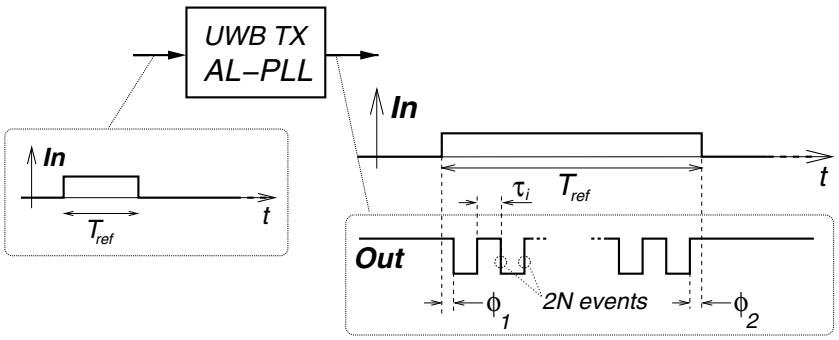

Fig. 4 All-digital pulse synthesis based on an asynchronous logic-phase locked loop (AL-PLL) (Bloor et al. 2005)

reference input. To generate a radio frequency pulse indeed, the circuit can be asynchronously triggered by the S-OOK modulator and, using ULP, it self-adjusts to generate a finite number of squared periods within the duty cycling reference input. The generated pulses have now a controlled center frequency and can be effectively radiated using an antenna with fixed selectivity. The asynchronous logic (AL) Duty cycled PLL generates a UWB pulse in the low FCC band (0–960 MHz) with a fractional bandwidth F larger than the minimum 0.2 required to radiate a UWB pulse. The AL-PLL UWB TX conceptual scheme is given in Fig. 4. As previously introduced in the system concept overview, the TX needs to be robust to RF center frequency variations, and needs to be self-adapted to large digital periods of the upstream logic. To synthesize controlled center frequency pulses at high frequency, the TX circuit is based on a single duty cycling reference input which can be very easily generated by the S-OOK modulator. The TX internally implements a feedback loop to lock this duty cycling reference input, and, using a Ring Oscillator, (the same circuit topology used to read-out sensor data), circuit architecture is maintained all-digital but generated signals are scaled to hundreds of MHz-order for over-the-air transmission. Based on T_{ref} pulse width, the circuit self adapts to synthesize a number of 2 N oscillations within a duty cycling duration. The synthesized RF signal is indeed 2 N times faster than $1/T_{ref}$, whose frequency is maintained very low, to aggressively save power consumption. The AL-PLL Impulse-Radio Transmitter is all-digital and scalable, therefore it can be easily implemented in lower technology nodes for higher and GHz-order center frequency operation and smaller antenna form factors. Alternatively to energy detection schemes, the TX can be combined with an asynchronous logic receiver which, based on its ULP features, can be even easily used in an MFC powered wireless sensor node (Crepaldi et al. 2013b).

3.4 Read-out circuit

The ROC used in this work is based on loading an all-digital RO. The circuit is implemented with discrete components (74HC00 logic gates) undersupplied to 1 V operation. Its operation principle is based on the propagation delay variation of the three-inverters chain based on both the resistive and capacitive properties of the material, which couples with the driving features of the output stage of the inverters. With larger applied pressure, the increased capacitance and resistance make RO frequency decrease, because it increases the propagation delay. The circuit is currently under characterization, it suits also other commercial pressure sensors still based on resistance and capacitance variation, and can be easily integrated in an ASIC.

4 Results and discussion

4.1 MFC subsystem

Beyond the measurements on the wireless sensor node reported further on, to test the MFC power generation we ran an electrochemical characterization on both single and 2 cells connected in series. All electrochemical experiments were run on a multi-channel VSP potentiostat (BioLogic) in a two-electrode set-up: a working and a counter-electrode, inserted on anode and cathode positions, respectively. Experiments regarded the measurements of the cell open circuit voltage, the current density, and sweep linear voltammetry. They were done to collect the information on the dynamics of the electron transfer too and, hence, on power generation. Polarization curves were measured at a scan rate of 0.1, 1 and 10 mV s^{-1}. Power was indirectly calculated by $P = I\,V$, where I and V are the recorded current and voltage outputs. Chronoamperometry was run at 0.1 and 0.6 V for monitoring the generated current. Furthermore, a third MFC (operating under the same conditions) was used to prove the capability of directly powering an array of 28 Light Emitting Diodes (LED, Avago HLMP-K150, low current double heterojunction AlGaAs/GaAs 637 nm dominant emission red lamp) and moreover to charge a supercapacitor (Maxwell, 1F, 2.7 V rated). The experiments were run at room temperature (24 ± 2 °C) in fed bath mode, using a Syringe Pump (NE-1600 Programmable Syringe Pump, USA) with hydraulic retention time (HRT) of 3 days for each MFC, feeding a synthetic

substrate at pH 7 and the organic loading rate of the carbon source, that is glucose of 0.5 g L^{-1} day^{-1}. MFCs are inoculated in the anode chamber by sea water (Arma di Taggia, Italy). The mixed culture, before to be fed in MFCs was previously enriched in batch in glass flasks in five following steps in anaerobic conditions (V inoculum 10 % of synthetic substrate, with the following composition in g L^{-1}: 10 $C_6H_{12}O_6$, 8.2 Na_2HPO_4, 5.2 NaH_2PO_4, 8 CH_3CO_2Na, 10 Peptone) in order to favorite microbial growth before inoculation in MFCs. The cathodic compartment was filled by potassium ferricyanide (6.58 g L^{-1}), added as oxidant compound, and a buffer solution of mineral salts Na_2HPO_4 (8.2 g L^{-1}) and NaH_2PO_4 (5.2 g L^{-1}) was used. Mixing is obtained through *recirculation* at high flow rate by multichannel peristaltic pumps at both anode and cathode chamber (Peri-Star Pro 4 and 8 channel (USA), respectively).

Figure 5 shows the (I,V) MFC polarization curves and power (P,V), obtained after 3-months of running test in stationary conditions. The curves are obtained using a Linear Sweep Voltammetry for a single MFC, immediately before the measurements session with the IR-UWB piezoresistive sensor node. Table 1 shows the results normalized with respect to volume and surface area: we obtained a maximum power density for two MFCs in series of 36 mW L^{-1} and 542 mW m^{-2}. These values remain stable for about 2 months of running tests, starting with an initial lag-phase, where the values were lower due to bacteria adaptation at the new conditions inside the anode chamber. Particularly, Table 1 shows that each MFC system is able to reach about 6.1 mW maximum power at 0.42 V of output supply voltage, against the few 0.7 mW absorbed by the MFC/IR-UWB piezo-resistive demonstrator. In any case, since the system needs a supply voltage of 1 ± 0.2 V, we used two MFCs connected in series. Anyway, these results demonstrate that an MFC system, properly dimensioned and stacked in series, could deliver enough power to supply a sensor node, taking into account both voltage and power absorption requirements. Figure 6 shows the output current at fixed output voltages of 0.1 and 0.6 V: even if current is higher at 0.1 V, we note a stabilization of the generated power at about 8 mW, whit 0.6 V. This finding is in accordance to the polarization curve depicted in Fig. 5 where the maximum power corresponds to 0.8 V.

As already mentioned, we tested two typical operational configurations too, one powering a string composed by 28 LEDs and one charging a supercapacitor. Results of the real-time MFC voltage drop and supercap charging are

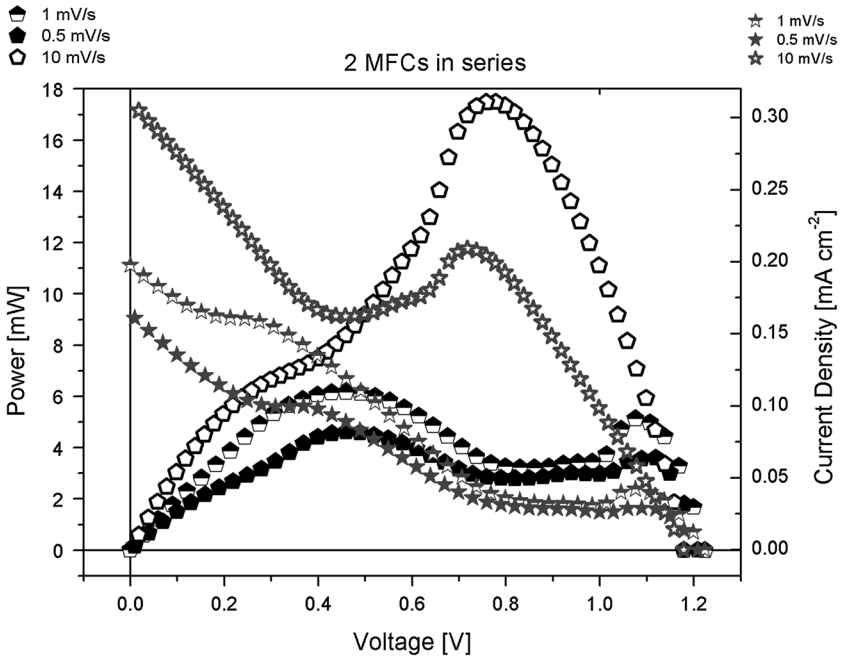

Fig. 5 Power and current density polarization curves produced by the MFCs in series, after 3 months of continuous running, for three different acquisition speeds: 0.5, 1 and 10 mV/s. Please note that only 1 point every 10, 50 and 20 respectively is shown for clarity

Table I Electrical properties measured from both singular MFC and MFC series assembly

MFC	Open circuit voltage (OCV) (V)	Maximum current (SCC) (mA m^{-2})	Power (mW)	Power density (mW m^{-2})	Power density (mW L^{-1})	Corresponding voltage-P_{max} (V)
MFC 1	0.58	1,280	4.9	427	28.4	0.49
MFC 2	0.71	4,228	8.9	784.75	52.2	0.36
Two MFC in series	1.22	1,978	6.1	542	36.1	0.42

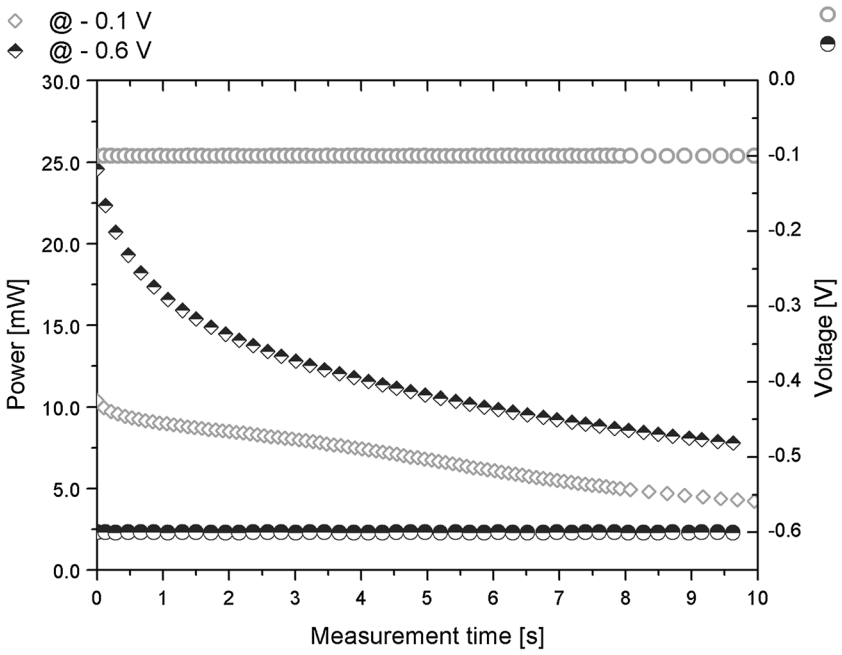

Fig. 6 Chronoamperometry at 0.1 and 0.6 V for the recovery of the corresponding output current

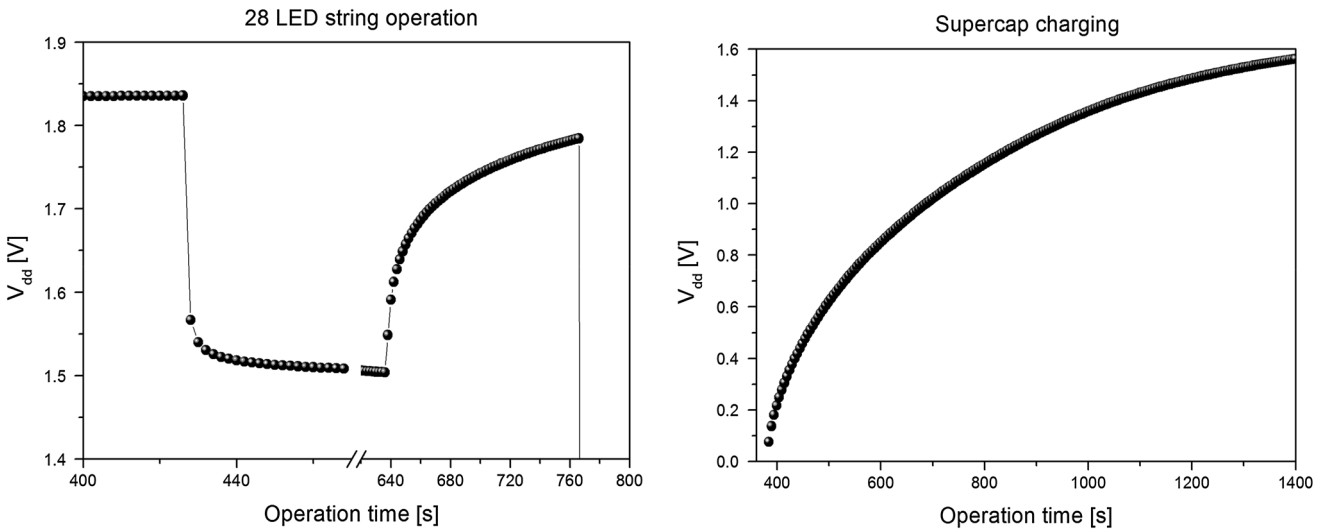

Fig. 7 MFC voltage drop measured in real-time during the switch-on and switch-off of a 28 LED string (*left*) and during a supercap charging (*right*)

shown in Fig. 7 left and right, respectively. Generally, the power output reported by many studies in literature is either based on the power dissipated on a static external resistor or is derived by means of voltammetry (e.g. linear sweep voltammetry or chronoamperometry). However, these measurements assume static conditions while it is clear that a real system normally operates in a dynamical environment, due to resources availability and load changes. We can in fact observe in Fig. 5 that the output power changes according to the voltammetry scan rate (0.1, 1, 10 ms^{-1}, respectively) and tends to grow, when scan rate increases. This implies inherent dynamic properties of the cell, which need to be accounted for an efficient design of the system. Through the tests with LEDs and supercapacitor we indeed directly obtained this information, i.e., by monitoring the current and voltage trends, through and across the MFC as a function of time. These preliminary tests are the starting point for future analyses on the dynamic properties of the cells and the necessary inputs to constrain downstream electronic circuits. This is the key of the presented project: the working characteristics of the supplying device (the MFC) are extracted, and the circuit is designed to be robust to the changes of the supply voltage, due to the dynamic behaviour of the MFC cell.

4.2 MFC-based wireless sensor node

Figure 8 shows the measurement set-up scheme for the combined MFC/IR-UWB and piezo-resistive demonstrator. In the set-up transmitted pulses are received by a high sampling rate oscilloscope with a connected antenna, emulating a receiver system. The measured T_p is a function of both the supply voltage V_{MFC} and, in our specific case, of the applied pressure on the sensor as well. The wireless sensor node is implemented in a Printed Circuit Board (PCB) which includes the integrated circuit comprising the TX and the discrete components read-out circuit. The supply terminals are directly connected to a series of two MFC, which provide an open circuit voltage of about 1.2 V. The piezoresistive sample connected to the ROC is loaded with finite bulk weight, for an overall pressure of 64 kPa.

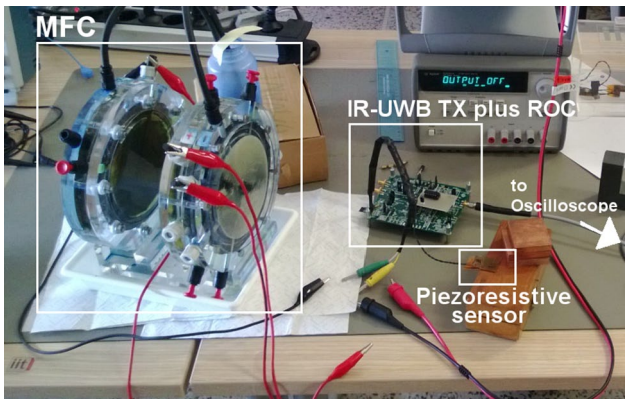

Fig. 8 Set-up scheme for the combined MFC/IR-UWB piezo-resistive demonstrator experiment (Crepaldi et al. 2013a)

Figure 9 shows the measured oscillation frequency $1/T_p$ as a function of the operation time and compares this curve to the available power in output from the MFC. The oscillation frequency $1/T_p$ is measured using a 4 GS/s oscilloscope (Agilent, DSO9404A). Pulses have center frequency of about 365 MHz, almost constant for the whole supply range, even if the TX duty cycling signal is far above the maximum limit. Results show that the oscillation period can be related to the power delivered by the MFC. In the experiment, as shown in Fig. 9, the absorbed power of the ROC plus the IR-UWB transmitter ranges from 630 to 725 μW: this is far below the maximum power achievable by the MFC. By comparing the power available from the MFC series assembly with the frequency shift after $1/T_p$ variation, a strong correlation is evident. By computing the correlation coefficient matrix on raw data we obtained 0.9095 (a correlation coefficient of 1 indicates that the raw data compared are either identical or proportional (Chiolerio et al. 2008).

We conclude that, with our test case, the ROC encodes pressure as a pulse rate variation, having an absolute sensitivity to the generated MFC voltage too, therefore correlating both signals. Once pressure information is digitally S-OOK modulated in a final prototype, S-OOK data rate can encode battery health and the pressure sensor can be, e.g., directly connected to the cells membrane and read excessive pressure level. Anyhow, the capability of wirelessly monitoring the voltage level available across the MFC, can enable the design of intelligent and "living" wireless sensor nodes, once a bidirectional transmitting and receiving functionality is implemented on each (Gorlatova et al. 2010). Based on the average pulse rate in fact, a transceiver WSN node, once a simple and low complexity

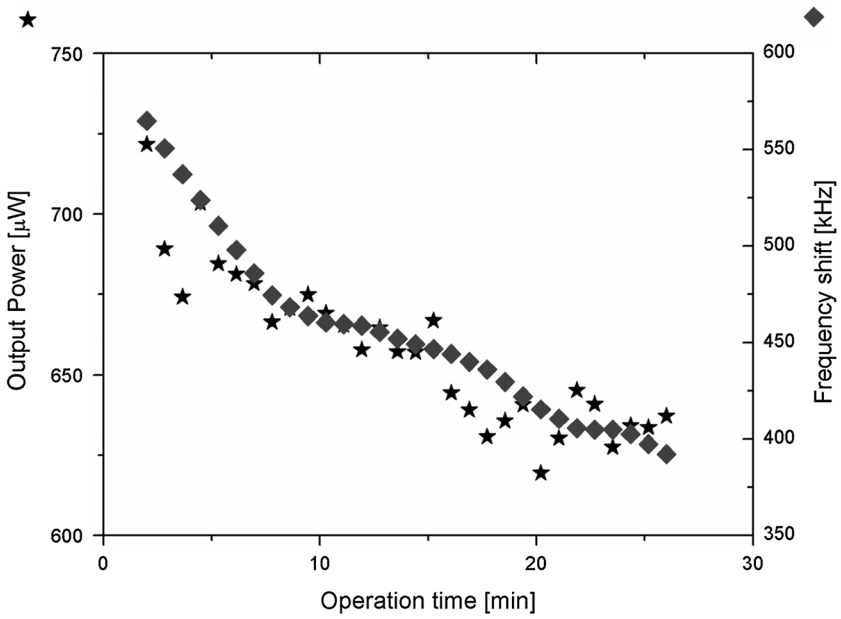

Fig. 9 A 30 min measurement session, with depicted MFC supply power, and the frequency corresponding to the oscillation period T_p of the transmitted signal, showing the good correlation between the two quantities

protocol is implemented in an ULP on-chip hardware, can sense each other supply conditions. Such a network will automatically self-adapt to hop information (or packets) across the energy healthy sensor nodes, and skip those with low MFC voltage level. This protocol would favour energy savings for those nodes whose environmental conditions are not suitable to feed microorganisms populating the MFC, i.e., to the maintenance of the complete network "healthy" and up-and-running.

Another innovative research field, which requires the strong interaction with electronic systems (in particular, adaptive energy management sub-systems), regards the implementation of a truly autonomous robot (EcoBot) that harvests energy from its environment, using MFCs as the onboard energy supply. The robot would digest organic matter such as food waste to transform these into useful electrical power. The low energy generated by the MFCs can then be stored in an on-board accumulator to be charged-up to a useful level, and then used to supply the robot sub-systems and run all the environmental tasks, e.g., measurement, data processing, communication and locomotion (Ieropoulos et al. 2008).

5 Conclusion

This work has reported on a wireless sensor node constrained on MFCs based on Impulse-Radio UWB for the transmission of the voltage level across a series of two microbial cells, plus an associated pressure level acquired using a piezoresistive nanostructured material and an associated read-out circuit. The paper has shown measurements and demonstrated feasibility on a first prototype including the most important subsystems. Our solution is all-digital and conceived to provide an efficient operation in environments where harvesting from wastewater is required. This is done without any energy management subsystems, providing potential power level monitoring capabilities to the sensor nodes.

References

Akyldiz I, Pompili D, Melodia T (2005) Underwater acoustic sensor networks: research challenges. Ad Hoc Netw 3:257–279

Bloor D, Donnelly K, Hands P et al (2005) A metal–polymer composite with unusual properties. J Phys D Apll Phys 38:2851–2860

Canavese G, Lombardi M, Stassi S, Pirri C (2012a) Comprehensive characterization of large piezoresistive variation of Ni-PDMS composites. Appl Mech Mater 110–116:1336–1344

Canavese G, Stassi S, Stralla M et al (2012b) Stretchable and conformable metal-polymer piezoresistive hybrid system. Sensors Actuators A Phys 186:191–197

Cheng S, Logan BE (2011) Increasing power generation for scaling up single-chamber air cathode microbial fuel cells. Bioresour Technol 102:4468–4473

Chiolerio A, Chiodoni A, Allia P (2008) Elemental distribution and morphological analysis of layered metallic systems: application to Co–Sn evaporated multilayers. Thin Solid Films 516:8453–8461

Chiolerio A, Roppolo I, Sangermano M (2013) Radical diffusion engineering: tailored nanocomposite materials for piezoresistive inkjet printed strain measurement. RSC Adv 3:3446–3452

Crepaldi M, Demarchi D (2013) A 130 nm CMOS 0.007 mm^2 ring oscillator-based self-calibrating IR-UWB transmitter using an asynchronous logic duty-cycled PLL. IEEE Trans Circuits Syst Express Briefs 60:237–241

Crepaldi M, Li C, Fernandes JR, Kinget PR (2011) An ultra-wideband impulse-radio transceiver chipset using synchronized-OOK modulation. IEEE J Solid State Circuits 46:2284–2299

Crepaldi M, Daprá D, Bonanno A et al (2012) Energy detection receivers. IEEE Trans Circuits Syst Regul Pap 59:2443–2455

Crepaldi M, Chiolerio A, Tommasi T et al (2013a) A low complexity wireless microbial fuel cell monitor using piezoresistive sensors and impulse-radio Ultra-Wide-Band. In: Proceedings of the SPIE 8763, Smart Sensors, Actuators, MEMS VI, 876311

Crepaldi M, Macis S, Motto Ros P, Demarchi D (2013b) A 0.07 mm^2 asynchronous logic CMOS pulsed receiver based on radio events self-synchronization. IEEE Trans Circuits Syst Regul Pap. (In press)

Di Lorenzo M, Curtis TP, Head IM, Scott K (2009) A single-chamber microbial fuel cell as a biosensor for wastewaters. Water Res 43:3145–3154

Diamond D, Coyle S, Scarmagnani S, Hayes J (2008) Wireless sensor networks and chemo-/biosensing. Chem Rev 108:652–679

Donovan C, Dewan A, Heo D, Beyenal H (2008) Batteryless, wireless sensor powered by a sediment microbial fuel cell. Environ Sci Technol 42:8591–8596

Eaton WPSJ (1997) Micromachined pressure sensors—review and recent developments. Smart Mater Struct 6:539

Gorlatova M, Kinget P, Kimissis I et al (2010) Energy harvesting active networked tags (EnHANTs) for Ubiquitous object networking. IEEE Wirel Commun 6:18–25

Guenther M, Gerlach G, Wallmersperger T (2010) Piezoresistive biochemical sensors based on hydrogels. Microsyst Technol 16:703–715

Ieropoulos I, Anderson I, Gisby T et al (2008) Microbial-powered artificial muscles for autonomous robots. Towar Auton Robot Syst Conf, pp 209–216

Jong B, Kim B, Cheng I et al (2006) Enrichment performance and microbial diversity of a thermophilic mediatorless microbial fuel cell. Environ Sci Technol 40:6449–6454

Logan BE (2010) Scaling up microbial fuel cells. Appl Microbio Biotechnol 85:1665–1671

Motto Ros P, Paleari M, Sanginario A et al (2013) A wireless address-event representation system for ATC-based multi-channel force wireless transmission. IWASI 2013:57–62

Müller M, Müller C, Gromball F et al (2003) Micro-structured flow fields for small fuel cells. Microsyst Technol 9:159–162

Park J-D, Ren Z (2012) Hysteresis-controller-based energy harvesting scheme for microbial fuel cells with parallel operation capability. Energy Convers IEEE Trans 27:715–724

Rabaey K, Verstraete W (2005) Microbial fuel cells: novel biotechnology for energy generation. Trends Biotechnol 23:291–298

Reimers CE, Girguis P, Stecher III HA et al (2006) Microbial fuel cell energy from an ocean cold seep. Geobiology 4:123–136

Ren H, Lee H, Chae J (2012) Miniaturizing microbial fuel cells for potential portable power sources: promises and challenges. Microfluid Nanofluid 13:353–381

Ruggeri B, Tommasi T (2012) Efficiency and efficacy of pre-treatment and bioreaction for bio-H 2 energy production from organic waste. Int J Hydrogen Energy 37:6491–6502

Ruggeri B, Bernardi M, Tommasi T (2012) On the pre-treatment of municipal organic waste towards fuel production: a review. Int J Environ Pollut 49:226–250

Stassi S, Canavese G, Cauda V et al (2012a) Evaluation of different conductive nanostructured particles as filler in smart piezoresistive composites. Nanoscale Res Lett 7:327–330

Stassi S, Canavese G, Cosiansi F et al (2012b) A tactile sensor device exploiting the tunable sensitivity of copper-PDMS piezoresistive composite. Procedia Eng 47:659–663

Stassi S, Cauda V, Canavese G et al (2012c) Synthesis and characterization of gold nanostars as filler of tunneling conductive polymer composites. Eur J Inorg Chem 16:2669–2673

Xie X, Ye M, Hu L et al (2012) Carbon nanotube-coated macroporous sponge for microbial fuel cell electrodes. Energy Environ Sci 5:5265–5270

Yousef H, Boukallel M, Althoefer KJ (2011) Tactile sensing for dexterous in-hand manipulation in robotics—a review. Sensors Actuators A Phys 2:171–187